AIMS Mathematics, 10(9): 22471–22496.
DOI: 10.3934/math.20251001
Received: 28 July 2025
Revised: 07 September 2025
Accepted: 15 September 2025
Published: 28 September 2025

https://www.aimspress.com/journal/Math

Research article

Bifurcation and solitary wave solutions of a time-dependent paraxial equation using improved modified extended tanh function method

Arooma Zainab[1], Muhammad Abbas[1,*], Yagoub A. S. Arko[2], Alina Alb Lupas[3,*], Tahir Nazir[1] and Muhammad Zain Yousaf[1]

[1] Department of Mathematics, University of Sargodha, Sargodha 40100, Pakistan
[2] Department of Mathematics, Turabah University College, Taif University, P.O. Box 11099, Taif 21944, Saudi Arabia
[3] Department of Mathematics and Computer Science, University of Oradea, Oradea 410087, Romania

* **Correspondence:** Email: muhammad.abbas@uos.edu.pk, dalb@uoradea.ro.

Abstract: This paper discusses an elaborate investigation of the dimensionless time-dependent paraxial equation based on its varied soliton solutions obtained through an improved modified extended tanh function method. The approach is capable of producing kink, bell-shaped, singular wave, periodic, singular periodic wave, bright and dark solitary wave, breather soliton, singular bell, M-shaped, W-shaped, and V-pattern solitons expressed as hyperbolic and trigonometric functions. Visualization via three dimensional (3D) surface plots, two dimensional (2D) cross-sections and contour plots allows a thorough examination of the wave morphology. Nonlinear dynamics are investigated using bifurcation, chaotic, sensitivity, and stability analyses that uncover complex solution behaviors and stability regimes. Modulation instability analysis verifies the stability of soliton structures under perturbations. The work demonstrates the effectiveness of the improved modified extended tanh function method for solving nonlinear partial differential equations and enhances theoretical knowledge of paraxial wave phenomena.

Keywords: improved modified extended tanh function method; dimensionless time-dependent paraxial equation; bifurcation; soliton solutions; stability
Mathematics Subject Classification: 34G20, 35A20, 35A22, 35R11

1. Introduction

Nonlinear partial differential equations (NLPDEs) are essential for modeling intricate phenomena in numerous real-world applications. They model heat conduction phenomena that are relevant for the

design of cooling systems and heat transfer optimization in industry. NLPDEs control the behavior of air and water flows in fluid dynamics and aerodynamics, contributing to aircraft, ship design, and weather forecasting. Electromagnetic fields and wireless communication systems depend on NLPDEs like Maxwell's equations to design antennas and radar systems. In biology, they describe population dynamics, disease epidemiology, and pattern formation. They are also applied in geology for seismic wave analyses and in environmental science to analyze pollutant dispersion and groundwater remediation. NLPDEs are central in financial mathematics to determine option prices and manage risks. Moreover, they enable image processing methods such as denoising and edge detection that improve medical imaging and satellite imagery. Their wide range of applications in engineering, physics, biology, finance, and environmental sciences underscores their importance to deciphering and resolving complex real–world issues. Here are some well-known NLPDEs [1, 2].

Several well-known NLPDEs have been under intense investigation for exact and analytical solutions via various classical and contemporary methodologies.Prominent among these are sine–Gordon equation [3] supports largespace, long-time kink-soliton gases, and multi-soliton (breather, kink, anti-kink) dynamics. The nonlinear Klein–Gordon equation [4] supports various bell-type, anti-bell, W-shaped, kink, anti-peakon, V-shaped, and flat soliton profiles, such as periodic and solitary-wave solutions. The Zoomeron equation [5] in the (2 + 1) space has provided kink, singular kink, periodic, and dark solitons, and travelling wave solutions. Furthermore, the (2 + 1)-dimensional Chaffee–Infante equation [6] allows for kink and cuspon soliton solutions, whereas its generalized version has rational, exponential, trigonometric, and hyperbolic soliton solutions. Such findings reflect the continued observation of complex wave phenomena like soliton gases, lumps, cuspons, and breathers in a series of cornerstone nonlinear wave models .

Analytical investigations mirror wider trends in the resolution of NLPDEs, where both symbolic and non-symbolic approaches are commonly employed. The sine-Gorden and sine–cosine expansion techniques [7, 8] have been extensively used to produce periodic and solitary wave solutions in many nonlinear models. The Hirota bilinear method [9] is a powerful symbolic tool for generating multi-soliton, lump, and rogue wave solutions in integrable systems. but it is typically restricted to bilinearization and often to integrable or near-integrable models. Moreover, the improved modified extended tanh method and other expansion techniques have been employed to obtain exact solutions for classical and fractional-order partial differential equations (PDEs) [10]. Conversely, non-symbolic techniques such as Wang's direct mapping technique are simple and efficient in mapping the solutions of auxiliary equations (e.g., Riccati) to the target PDE [11] without complex symbolic computations. Although more rapid, such techniques might lack new wave structures without initial ansatz assumptions, stressing the benefit of more systematic symbolic expansions, such as in the present work. Liang and Wang [12] obtained new exact solutions of the local fractional Vakhnenko–Parkes equation on the basis of high-order fractional calculus methods. Their research indicates the complex dynamics and stability characteristics of nonlinear waves in fractal media, expanding classical models to fractional orders.

In this present research, the improved modified extended tanh function method (IMETFM) is used to obtain analytical solutions of the dimensionless time-dependent paraxial (DTDP) equation by converting its nonlinear form into more tractable auxiliary equations. This method is intended to broaden the range of possible solutions of the DTDP equation and improve the understanding of its highly nonlinear behavior. The IMETFM is a robust analytical approach to find traveling

wave solutions of NLPDEs. By representing solutions as series expansions with hyperbolic tangent functions and solving the corresponding Riccati equations, the method has ability to produce various solutions, such as bright/dark solitons, periodic waves, and rational or exponential functions. It has been extensively used for families of equations like three dimensional(3D) fractional Wazwaz–Benjamin–Bona–Mahony (WBBM) equations and Boussinesq equations, for which it uncovered soliton interactions, and multi-wave structures and produced Jacobi/Weierstrass doubly periodic elliptic solutions. The strength of the method lies in its controlled reduction of PDEs into algebraic systems by wave transformations, allowing exact parameter relations. New extensions show its flexibility for handling problems like the generalized Ito equations, generating kinks and plane periodic solutions. Major developments of the IMETFM were made by Yang and Hon, and their work continues to provide a base for recent applications in nonlinear wave dynamics. The IMETFM has also been effectively used to obtain soliton and traveling wave solutions of intricate nonlinear equations, such as high-order nonlinear Schrödinger [13] and fractional-order Fokas equations. The research emphasizes the efficacy of the method in describing various wave phenomena in both integer and fractional nonlinear models [14–16].

The DTDP equation, has been a central focus in nonlinear optics to describe the propagation of electromagnetic waves in Kerr media. New research has greatly improved the DTDP equation's understanding and solution techniques in complex and dynamic environments. Gomez [17] proposed a fractional DTDP equation to describe wave-front propagation in randomly layered media with long-range correlations, which preserves the non local effects using multiscale analysis. Akram et al. [18] used the extended hyperbolic function method to derive exact soliton solutions, which improved the range of analytically available solutions. Tarla and Yilmazer [19] analyzed the DTDP equation with analytical methods, obtaining solutions for time-dependent refractive indices. They subsequently developed a modified unified auxiliary equation method (MUAEM), enhancing the solution's diversity and flexibility [20]. Tun [21] obtained optical soliton solutions of the DTDP equation and performed stability analysis, determining the conditions for stable propagation. Collectively, these studies embody a double movement: Universalizing the DTDP equation to realistic media and the improvement of analytical approaches for precise solutions [22].

Bifurcation analysis has been used widely in nonlinear evolution equations like the fractional complex Ginzburg–Landau equation [23] and its extensions with Kerr and parabolic law nonlinearities to identify the critical parameter values at which the system switches between multiple wave behaviors. Classification of various exact traveling wave solutions like compactons and bounded waves with degenerate equilibria and nonanalytic vector fields is made possible through this method. The Ginzburg–Landau theory is also a paradigm for bifurcation phenomena in manifolds, with eigenvalues of Laplace-type operators determining the bifurcation points. These investigations bypass difficulties associated with singular traveling wave systems and complex elliptic integrals and shed light on the intricate solution structures and stability features. In addition, the bifurcation theory of the corresponding PDEs such as nonlinear Kodama and fractional WBBM equations reveals transitions to chaotic and quasi-periodic behavior, and sensitivity analyses reveal how slight parameter changes affect the solutions's stability. In total, bifurcation and sensitivity analyses of these classic PDEs enhance our understanding of nonlinear wave propagation, pattern formation, and intricate dynamical behaviors in fractional and classical models [24–26].

The principal objective of this paper is to apply the IMETFM to the DTDP equation to derive new

analytical solutions. Particular attention is paid to explore rich soliton structures, such as kink, bell-shaped, singular wave, periodic, singular periodic wave, bright and dark solitary wave, breather soliton, singular bell, M-shaped, W-shaped, and V-pattern soliton solutions. Bifurcation analysis is carried out in order to study the qualitative change in the solution's behavior that results from variations in the system parameters and may eventually cause chaotic dynamics and illustrate system sensitivity. The stability of the solutions is independently analyzed through the addition of perturbation terms. This methodology expands the reachable solution space of the DTDP equation and increases our knowledge of its nonlinear wave dynamics. The research also shows the efficacy of the IMETFM to solve multidimensional NLPDEs with intricate behaviors. In general, the approach is able to capture bifurcation, chaos, sensitivity, and stability phenomena in the DTDP model.

Motivation for this research arises from the necessity to investigate NLPDEs that model wave dynamics in telecommunication systems, plasma, fluids, and optics. The DTDP equation has not been thoroughly investigated, with the existing literature focusing on only a few solitons. To bridge this research gap, the IMETFM is used to derive various new soliton solutions that are stable and physically interpretable. Bifurcation, chaos, and sensitivity behaviors are also studied. These findings provide the analytical insights into nonlinear wave's evolution in realistic systems.

The paper is structured as follows: Section 2 shows the detail about the model. In Section 3, the DTDP equation is reduced to an ordinary differential equation (ODE). Section 4 show the descriptions of the IMETFM. Diverse soliton solutions of the DTDP equation are obtained through the IMETFM in Section 5, and the dynamic behaviors of these solutions in 3D, two dimensional(2D) and contour plots are displayed in Section 6. Phase portraits and bifurcation behavior analysis of the DTDP equation are described in Section 7. Chaotic behavior with respect to the DTDP equation is presented in Section 8, and an anlysis of sensitivity to the initial values is described in Section 9. The physical interpretation of the solutions is discussed in Section 10. Comparisons, advantages, and limitations are described in Section 11. The stability of the model is described in Section 12. The conclusions are presented in Section 13.

2. Governing equation

Let us examine the following DTDP model as:

$$i\Psi_y + \frac{\alpha}{2}\Psi_{tt} + \frac{\beta}{2}\Psi_{xx} + \gamma|\Psi|^2\Psi = 0, \tag{2.1}$$

where wave characteristic is represented by the associated complex-valued component $\Psi = \Psi(x, y, t)$. The dimensions in Eq (2.1) are reflected by the factors x, y, and t correspondingly and the constraints of Eq (2.1) are α, β, and γ.

3. Wave transformation

We utilized the traveling wave transforms outlined below to take advantage of the phase-amplitude structure:

$$\begin{cases} \Psi(x, y, t) = Z(\xi)e^{i(ax+by-ct)}, \\ \xi = x + y - \mu t, \end{cases} \tag{3.1}$$

where, $Z(\xi)$ is used to denote the soliton's speed, and also describes the fundamental structure of the wave profile. At the same time, the parameters a, b, c, and μ can be used to define the soliton, soliton wave number, and a phase parameter. After substituting Eq (3.1) into Eq (2.1), the resulting ODE is as follows:

$$(-b - \frac{c^2\alpha}{2} - \frac{a^2\beta}{2})Z + \gamma Z^3 + (\frac{\mu^2\alpha}{2} + \frac{\beta}{2})Z'' + 2i(1 + \mu c\alpha + a\beta)Z' = 0 \tag{3.2}$$

setting imaginary part of Eq (3.2) equal to zero, which gives $\mu = \frac{-1-a\beta}{c\alpha}$,

$$(-b - \frac{c^2\alpha}{2} - \frac{a^2\beta}{2})Z + \gamma Z^3 + (\frac{\mu^2\alpha}{2} + \frac{\beta}{2})Z'' = 0. \tag{3.3}$$

4. Algorithm of the IMETFM

This is a discussion of how to apply the IMETFM in order to achieve soliton solutions for DTDP equation. Consider the following NLPDE with three independent variables x, y, and t:

$$A(\Psi, \Psi_x, \Psi_t, \Psi_y, \Psi_{xx}, \Psi_{tt}, \ldots) = 0, \tag{4.1}$$

as discussed earlier Eq (4.1), Ψ is an unknown function and A is the polynomial that has Ψ. The indices here correspond to its partial derivatives with respect to x, y, and t and these are nonlinear components and highest-order derivatives. The following steps demonstrate the IMETFM's guidelines.

Step 1. Taking the following wave transformation:

$$\Psi(x, y, t) = Z(\xi)e^{i(ax+by-ct)}, \tag{4.2}$$

where $\xi = x + y - \mu t$. The solutions can be found by switching Eq (4.1) to the resulting ODE and using the wave translation given in Eq (4.2).

$$B(Z, Z', Z'', \ldots) = 0, \tag{4.3}$$

where $'$ controls the derivative based on ξ, which indicates that B is a polynomial expression in $Z(\xi)$ together with the derivatives corresponding to both of them, e.g., $Z'(\xi) = \frac{dZ}{d\xi}$, $Z''(\xi) = \frac{d^2Z}{d\xi^2}$, etc.

Step 2. Consider the following structure to be the solution to Eq (4.3):

$$Z(\xi) = \sum_{i=0}^{N} r_i\eta^i(\xi) + \sum_{j=1}^{N} s_j\eta^{-j}(\xi), \tag{4.4}$$

where N represents an unknown numerical parameter. To determine the unchanging component, the values of r_i and s_j are used. For this unknown factor to be zero at the same time is not rational. The $Z(\xi)$ is determined in the following manner:

$$Z'(\xi) = \epsilon\sqrt{m_0 + m_1\eta(\xi) + m_2\eta(\xi)^2 + m_3\eta(\xi)^3 + m_4\eta(\xi)^4}, \tag{4.5}$$

where m_0, m_1, m_2, m_3, and m_4 are constants and $\epsilon = \pm 1$.

Step 3. It is simple to determine the value of N used in the solution (4.4) by finding the homogeneous balance method between linear and nonlinear components with the most substantial order provided in

Eq (4.3).

Step 4. With the use of Eq (4.5), the result of (4.4) may be translated into Eq (4.3) to yield a polynomial in $Z(\xi)$. The algebraic system can therefore be achieved by comparing the coefficient of $\eta^i(\xi)$. After handling the previously given algebraic equation structures in Mathematica 13.3, the crucial fixing factors r_i and s_j can be found.

Step 5. Several types of solutions can be obtained by assigning a large number of possible choices for r_0, r_1, and s_1. There are six following cases of the IMETFM.

Case 1: If $m_0 = m_1 = m_3 = 0$, then the following solutions are obtained:

$$\eta_1(\xi) = \sqrt{-\frac{m_2}{m_4}}\,\operatorname{sech}\left(\sqrt{m_2}\,\xi\right), \quad m_2 > 0, \quad m_4 < 0,$$

$$\eta_2(\xi) = \sqrt{-\frac{m_2}{m_4}}\,\sec\left(\sqrt{m_2}\,\xi\right), \quad m_2 < 0, \quad m_4 > 0,$$

$$\eta_3(\xi) = -\frac{\epsilon}{\sqrt{m_4}\,\xi}, \quad m_2 = 0, \quad m_4 > 0.$$

Case 2: If $m_1 = m_3 = 0$, then the following solutions are obtained:

$$\eta_4(\xi) = \sqrt{-\frac{m_2}{2m_4}}\,\tanh\left(\sqrt{-\frac{m_2}{2}}\,\xi\right), \quad m_2 < 0, \quad m_0 = \frac{m_2^2}{4m_4}, \quad m_4 > 0,$$

$$\eta_5(\xi) = \sqrt{\frac{m_2}{2m_4}}\,\tan\left(\sqrt{\frac{m_2}{2}}\,\xi\right), \quad m_2 > 0, \quad m_0 = \frac{m_2^2}{4m_4}, \quad m_4 > 0,$$

$$\eta_6(\xi) = \sqrt{-\frac{m_2\,n^2}{m_4\,(2n^2-1)}}\,\operatorname{cn}\left(\sqrt{\frac{m_2\,n^2}{2n^2-1}}\,\xi\right), \quad m_2 > 0, \quad m_0 = \frac{m_2^2\,n^2(1-n^2)}{m_4\,(2n^2-1)^2}, \quad m_4 < 0,$$

$$\eta_7(\xi) = \sqrt{-\frac{n^2}{m_4\,(2-n^2)}}\,\operatorname{dn}\left(\sqrt{\frac{m_2}{2-n^2}}\,\xi\right), \quad m_2 > 0, \quad m_0 = \frac{m_2^2\,(1-n^2)}{m_4\,(2-n^2)^2}, \quad m_4 < 0,$$

$$\eta_8(\xi) = \sqrt{-\frac{m_2\,n^2}{m_4\,(n^2+1)}}\,\operatorname{sn}\left(\sqrt{-\frac{m_2}{n^2+1}}\,\xi\right), \quad m_2 < 0, \quad m_0 = \frac{m_2^2\,n^2}{m_4\,(n^2+1)^2}, \quad m_4 > 0.$$

Case 3: If $m_2 = m_4 = 0$, then the following solution is obtained:

$$\eta_9(\xi) = \wp\left(\frac{\sqrt{m_3}\,\xi}{2}, -\frac{4m_1}{m_3}, -\frac{4m_0}{m_3}\right), \quad m_3 > 0, \quad m_0 \neq 0, \quad m_1 \neq 0.$$

Case 4: If $m_0 = m_1 = m_2 = 0$, then the following solutions are obtained:

$$\eta_{10}(\xi) = \frac{4m_3}{m_3^2\xi^2 - 4m_4}, \quad m_4 \neq 0,$$

$$\eta_{11}(\xi) = \frac{m_3\,e^{\frac{\epsilon m_3 \xi}{2\sqrt{-m_4}}}}{2m_4}, \quad m_4 < 0.$$

Case 5: If $m_3 = m_4 = 0$, then the following solutions are obtained:

$$\eta_{12}(\xi) = \sqrt{-\frac{m_0}{m_2}}\ \sin\left(\sqrt{-m_2}\,\xi\right), \quad m_1 = 0, \quad m_2 < 0, \quad m_0 > 0,$$

$$\eta_{13}(\xi) = \sqrt{\frac{m_0}{m_2}}\ \sinh\left(\sqrt{-m_2}\,\xi\right), \quad m_1 = 0, \quad m_2 < 0, \quad m_0 > 0,$$

$$\eta_{14}(\xi) = e^{\epsilon\sqrt{m_2}\,\xi} - \frac{m_1}{2m_2}, \quad m_0 = \frac{m_1^2}{4m_2}, \quad m_2 > 0.$$

Case 6: If $m_0 = m_1 = 0$ and $m_4 > 0$, then the following solutions is obtained:

$$\eta_{15}(\xi) = \frac{\epsilon}{2}\sqrt{\frac{m_2}{m_4}}\left(\tanh\left(\frac{\sqrt{m_2}\,\xi}{2}\right) + 1\right), \quad m_3 = 2\epsilon\sqrt{m_2 m_4}, \quad m_2 > 0.$$

5. Implementation of the IMETFM

This section looks at how the IMETFM is used to analyze the DTDP model. When Z^3 is balanced with respect to Z'' in Eq (3.3), $N = 1$ is the result. Accordingly, Eq (4.4) corresponds to,

$$Z(\xi) = r_0 + r_1\eta(\xi) + \frac{s_1}{\eta(\xi)}. \tag{5.1}$$

The following structure uses Eq (4.1) and the solution (4.5) to find the polynomial in the form of $Z(\xi)$ for Eq (3.3):

$$\begin{cases} -4\beta\epsilon^2 m_0 s_1 - 4\alpha\epsilon^2\mu^2 m_0 s_1 - 4\gamma s_1^3 - 3\beta\epsilon^2 m_1 s_1\eta(\xi) - 3\alpha\epsilon^2\mu^2 m_1 s_1\eta(\xi) \\ -12\gamma r_0^2 s_1\eta(\xi) + 4bs_1\eta(\xi)^2 + 2c^2\alpha s_1\eta(\xi)^2 + 2a^2\beta s_1\eta(\xi)^2 - 2\beta\epsilon^2 m_2 s_1\eta(\xi)^2 - 2\alpha\epsilon^2\mu^2 m_2 s_1\eta(\xi)^2 \\ -12\gamma r_0^2 s_1\eta(\xi)^2 - 12\gamma r_1 s_1^2\eta(\xi)^2 + 4br_0\eta(\xi)^3 + 2c^2\alpha r_0\eta(\xi)^3 + 2a^2\beta r_0\eta(\xi)^3 - 4\gamma r_0^3\eta(\xi)^3 \\ -\beta\epsilon^2 m_1 r_1\eta(\xi)^3 - \alpha\epsilon^2\mu^2 m_1 r_1\eta(\xi)^3 - \beta\epsilon^2 m_3 s_1\eta(\xi)^3 \\ -\alpha\epsilon^2\mu^2 m_3 s_1\eta(\xi)^3 - 24\gamma r_0 r_1 s_1\eta(\xi)^3 + 4br_1\eta(\xi)^4 \\ +2c^2\alpha r_1\eta(\xi)^4 + 2a^2\beta r_1\eta(\xi)^4 - 2\beta\epsilon^2 m_2 r_1\eta(\xi)^4 - 2\alpha\epsilon^2\mu^2 m_2 r_1\eta(\xi)^4 \\ -12\gamma r_0^2 r_1\eta(\xi)^4 - 12\gamma r_1^2 s_1\eta(\xi)^4 - 3\beta\epsilon^2 m_3 r_1\eta(\xi)^5 - 3\alpha\epsilon^2\mu^2 m_3 r_1\eta(\xi)^5 \\ -12\gamma r_0 r_1^2\eta(\xi)^5 - 4\beta\epsilon^2 m_4 r_1\eta(\xi)^6 - 4\alpha\epsilon^2\mu^2 m_4 r_1\eta(\xi)^6 - 4\gamma r_1^3\eta(\xi)^6 = 0. \end{cases} \tag{5.2}$$

With a comparable dimension of $\eta(\xi)$ equal to zero, Eq (5.2) can be used to construct the whole range of algebraic equations.

$$\begin{cases} (\eta(\xi))^0 : -4\beta\epsilon^2 m_0 s_1 - 4\alpha\epsilon^2\mu^2 m_0 s_1 - 4\gamma s_1^3, \\ (\eta(\xi))^1 : -3\beta\epsilon^2 m_1 s_1 - 3\alpha\epsilon^2\mu^2 m_1 s_1 - 12\gamma r_0 s_1^2, \\ (\eta(\xi))^2 : 4bs_1 + 2c^2\alpha s_1 + 2a^2\beta s_1 - 2\beta\epsilon^2 m_2 s_1 - 2\alpha\epsilon^2\mu^2 m_2 s_1 - 12\gamma r_0^2 s_1 - 12\gamma r_1 s_1^2, \\ (\eta(\xi))^3 : 4br_0 + 2c^2\alpha r_0 + 2a^2\beta r_0 - 4\gamma r_0^3 - \beta\epsilon^2 m_1 r_1 - \alpha\epsilon^2\mu^2 m_1 r_1 - \beta\epsilon^2 m_3 s_1 - \alpha\epsilon^2\mu^2 m_3 s_1 - 24\gamma r_0 r_1 s_1, \\ (\eta(\xi))^4 : 4br_1 + 2c^2\alpha r_1 + 2a^2\beta r_1 - 2\beta\epsilon^2 m_2 r_1 - 2\alpha\epsilon^2\mu^2 m_2 r_1 - 12\gamma r_0^2 r_1 - 12\gamma r_1^2 s_1, \\ (\eta(\xi))^5 : -3\beta\epsilon^2 m_3 r_1 - 3\alpha\epsilon^2\mu^2 m_3 r_1 - 12\gamma r_0 r_1^2, \\ (\eta(\xi))^6 : -4\beta\epsilon^2 m_4 r_1 - 4\alpha\epsilon^2\mu^2 m_4 r_1 - 4\gamma r_1^3. \end{cases}$$

Solving the system of equations above by using Mathematica 13.3 software gives the following.
Case 1: If $m_0 = m_1 = m_3 = 0$, then it gives

$$r_0 = 0, \quad s_1 = 0, \quad r_1 = \frac{i\epsilon\sqrt{\beta+\alpha\mu^2}\sqrt{m_4}}{\sqrt{\gamma}}, \quad m_2 = \frac{2b+c^2\alpha+a^2\beta}{\epsilon^2(\beta+\alpha\mu^2)},$$

and the following solutions:

$$\Psi_1(\xi) = \frac{ie^{i(-tc+ax+by)}\epsilon\sqrt{\beta+\alpha\mu^2}\,\operatorname{sech}\left(\sqrt{\frac{2b+c^2\alpha+a^2\beta}{\epsilon^2(\beta+\alpha\mu^2)}}\,\xi\right)\sqrt{-\frac{2b+c^2\alpha+a^2\beta}{\epsilon^2(\beta+\alpha\mu^2)}}}{\sqrt{\gamma}}, \tag{5.3}$$

$$\Psi_2(\xi) = \frac{ie^{i(-tc+ax+by)}\epsilon\sqrt{\beta+\alpha\mu^2}\,\sec\left(\sqrt{-\frac{2b+c^2\alpha+a^2\beta}{\epsilon^2(\beta+\alpha\mu^2)}}\,\xi\right)\sqrt{-\frac{2b+c^2\alpha+a^2\beta}{\epsilon^2(\beta+\alpha\mu^2)}}}{\sqrt{\gamma}}, \tag{5.4}$$

$$\Psi_3(\xi) = -\frac{ie^{i(-tc+ax+by)}\epsilon^2\sqrt{\beta+\alpha\mu^2}}{\sqrt{\gamma}\,\xi}. \tag{5.5}$$

Case 2: If $m_1 = m_3 = 0$, then it gives

$$r_0 = 0, \quad s_1 = 0, \quad r_1 = \pm\frac{i\epsilon\sqrt{\beta+\alpha\mu^2}\sqrt{m_4}}{\sqrt{\gamma}}, \quad m_2 = \frac{2b+c^2\alpha+a^2\beta}{\epsilon^2(\beta+\alpha\mu^2)},$$

and the following solutions:

$$\Psi_4(\xi) = \frac{ie^{i(-ct+ax+by)}\epsilon\sqrt{\beta+\alpha\mu^2}\sqrt{-\frac{2b+c^2\alpha+a^2\beta}{\epsilon^2(\beta+\alpha\mu^2)}}\tanh\left(\frac{\sqrt{-\frac{2b+c^2\alpha+a^2\beta}{\epsilon^2(\beta+\alpha\mu^2)}}\,\xi}{\sqrt{2}}\right)}{\sqrt{2}\sqrt{\gamma}}, \tag{5.6}$$

$$\Psi_5(\xi) = \frac{ie^{i(-ct+ax+by)}\epsilon\sqrt{\beta+\alpha\mu^2}\sqrt{\frac{2b+c^2\alpha+a^2\beta}{\epsilon^2(\beta+\alpha\mu^2)}}\tan\left(\frac{\sqrt{\frac{2b+c^2\alpha+a^2\beta}{\epsilon^2(\beta+\alpha\mu^2)}}\,\xi}{\sqrt{2}}\right)}{\sqrt{2}\sqrt{\gamma}}, \tag{5.7}$$

$$\Psi_6(\xi) = \frac{ie^{i(-ct+ax+by)}\epsilon\sqrt{\beta+\alpha\mu^2}\,\operatorname{cn}\left(\sqrt{\frac{n^2(2b+c^2\alpha+a^2\beta)}{(-1+2n^2)\epsilon^2(\beta+\alpha\mu^2)}}\,\xi, n\right)\sqrt{-\frac{n^2(2b+c^2\alpha+a^2\beta)}{(-1+2n^2)\epsilon^2(\beta+\alpha\mu^2)}}}{\sqrt{\gamma}}, \tag{5.8}$$

$$\Psi_7(\xi) = \frac{ie^{i(-ct+ax+by)}\epsilon\sqrt{\beta+\alpha\mu^2}\,\operatorname{dn}\left(\sqrt{\frac{2b+c^2\alpha+a^2\beta}{(2-n^2)\epsilon^2(\beta+\alpha\mu^2)}}\,\xi, n\right)\sqrt{-\frac{n^2}{2-n^2}}}{\sqrt{\gamma}}, \tag{5.9}$$

$$\Psi_8(\xi) = \frac{ie^{i(-ct+ax+by)}\epsilon\sqrt{\beta+\alpha\mu^2}\,\operatorname{sn}\left(\sqrt{-\frac{2b+c^2\alpha+a^2\beta}{(1+n^2)\epsilon^2(\beta+\alpha\mu^2)}}\,\xi, n\right)\sqrt{-\frac{n^2(2b+c^2\alpha+a^2\beta)}{(1+n^2)\epsilon^2(\beta+\alpha\mu^2)}}}{\sqrt{\gamma}}. \tag{5.10}$$

Case 3: If $m_2 = m_4 = 0$, then it gives

$$r_0 = \frac{\sqrt{2b + c^2\alpha + a^2\beta}}{\sqrt{2}\,\sqrt{\gamma}},\ s_1 = -\frac{\epsilon^2(\beta + \alpha\mu^2)m_1}{4\gamma r_0},\ r_1 = 0,$$
$$m_0 = -\frac{3\epsilon^2(\beta + \alpha\mu^2)m_1^2}{8(2b + c^2\alpha + a^2\beta)},\ m_3 = -\frac{8(2b + c^2\alpha + a^2\beta)^2}{9\epsilon^4(\beta + \alpha\mu^2)^2 m_1},$$

and the following solution:

$$\Psi_9(\xi) = -\frac{e^{-i(-ct+ax+by)}\,\epsilon^2(\beta + \alpha\mu^2)\,m_1}{2\sqrt{2}\,\sqrt{2b + c^2\alpha + a^2\beta}\,\sqrt{\gamma}\,\wp\left(\frac{1}{3}\sqrt{2}\xi\sqrt{-\frac{(2b+c^2\alpha+a^2\beta)^2}{\epsilon^4(\beta+\alpha\mu^2)^2 m_1}}, \frac{9\epsilon^4(\beta+\alpha\mu^2)^2 m_1^2}{2(2b+c^2\alpha+a^2\beta)^2}, -\frac{27\epsilon^6(\beta+\alpha\mu^2)^2(\beta+\alpha\mu^2)m_1^3}{16(2b+c^2\alpha+a^2\beta)^3}\right)}$$
$$+ \frac{\sqrt{2b + c^2\alpha + a^2\beta}}{\sqrt{2}\,\sqrt{\gamma}}. \tag{5.11}$$

Case 4: If $m_0 = m_1 = m_2 = 0$, then it gives

$$r_0 = \frac{\sqrt{2b + c^2\alpha + a^2\beta}}{\sqrt{2}\,\sqrt{\gamma}}, \quad s_1 = 0, \quad r_1 = \frac{i\epsilon\sqrt{\beta + \alpha\mu^2}\,\sqrt{m_4}}{\sqrt{\gamma}}$$

and the following solutions:

$$\Psi_{10}(\xi) = \frac{\sqrt{2b + c^2\alpha + a^2\beta}}{\sqrt{2}\,\sqrt{\gamma}} + \frac{4ie^{i(-ct+ax+by)}\,\epsilon\sqrt{\beta + \alpha\mu^2}\,m_3\,\sqrt{m_4}}{\sqrt{\gamma}\left(\xi^2 m_3^2 - 4m_4\right)}, \tag{5.12}$$

$$\Psi_{11}(\xi) = \frac{\sqrt{2b + c^2\alpha + a^2\beta}}{\sqrt{2}\,\sqrt{\gamma}} + \frac{i\,e^{i(-ct+ax+by)+\frac{\epsilon\xi m_3}{2\sqrt{-m_4}}}\,\epsilon\sqrt{\beta + \alpha\mu^2}\,m_3}{2\sqrt{\gamma}\,\sqrt{m_4}}. \tag{5.13}$$

Case 5: If $m_3 = m_4 = 0$, then it gives

$$r_0 = \frac{\sqrt{2b + c^2\alpha + a^2\beta}}{\sqrt{2}\,\sqrt{\gamma}}, \quad s_1 = \frac{i\epsilon\sqrt{\beta + \alpha\mu^2}\,\sqrt{m_0}}{\sqrt{\gamma}}, \quad r_1 = 0, \quad m_2 = \frac{2b + c^2\alpha + a^2\beta - 6\gamma r_0^2 - 6\gamma r_1 s_1}{\epsilon^2(\beta + \alpha\mu^2)},$$

and the following solutions:

$$\Psi_{12}(\xi) = \frac{\sqrt{2b + c^2\alpha + a^2\beta}}{\sqrt{2}\,\sqrt{\gamma}} + \frac{ie^{-i(-ct+ax+by)}\,\epsilon\sqrt{\beta + \alpha\mu^2}\,csch\left(\sqrt{-\frac{2b+c^2\alpha+a^2\beta-3(2b+c^2\alpha+a^2\beta)}{\epsilon^2(\beta+\alpha\mu^2)}}\,\xi\right)\sqrt{m_0}}{\sqrt{\gamma}\,\sqrt{\frac{\epsilon^2(\beta+\alpha\mu^2)m_0}{2b+c^2\alpha+a^2\beta-3(2b+c^2\alpha+a^2\beta)}}}, \tag{5.14}$$

$$\Psi_{13}(\xi) = \frac{\sqrt{2b + c^2\alpha + a^2\beta}}{\sqrt{2}\,\sqrt{\gamma}} + \frac{ie^{-i(-ct+ax+by)}\,\epsilon\sqrt{\beta + \alpha\mu^2}\,\csc\left(\sqrt{-\frac{2b+c^2\alpha+a^2\beta-3(2b+c^2\alpha+a^2\beta)}{\epsilon^2(\beta+\alpha\mu^2)}}\,\xi\right)\sqrt{m_0}}{\sqrt{\gamma}\,\sqrt{-\frac{\epsilon^2(\beta+\alpha\mu^2)m_0}{2b+c^2\alpha+a^2\beta-3(2b+c^2\alpha+a^2\beta)}}}, \tag{5.15}$$

$$\Psi_{14}(\xi) = \frac{\sqrt{2b + c^2\alpha + a^2\beta}}{\sqrt{2}\,\sqrt{\gamma}} + \frac{ie^{-i(-ct+ax+by)}\,\epsilon\sqrt{\beta + \alpha\mu^2}\,\sqrt{m_0}}{\sqrt{\gamma}\left(e^{\epsilon\sqrt{\frac{2b+c^2\alpha+a^2\beta-3(2b+c^2\alpha+a^2\beta)}{\epsilon^2(\beta+\alpha\mu^2)}}\,\xi} - \frac{\epsilon^2(\beta+\alpha\mu^2)m_1}{2(2b+c^2\alpha+a^2\beta-3(2b+c^2\alpha+a^2\beta))}\right)}. \tag{5.16}$$

Case 6: If $m_0 = m_1 = 0$ and $m_4 > 0$, then it gives

$$r_0 = \frac{\sqrt{2b + c^2\alpha + a^2\beta}}{\sqrt{2}\sqrt{\gamma}}, \quad r_1 = \frac{i\epsilon\sqrt{\beta + \alpha\mu^2}\sqrt{m_4}}{\sqrt{\gamma}}, \quad s_1 = 0, \quad m_2 = \frac{2b + c^2\alpha + a^2\beta - 6\gamma r_0^2 - 6\gamma r_1 s_1}{\epsilon^2(\beta + \alpha\mu^2)}$$

and the following solution:

$$\Psi_{15}(\xi) = \left(1 + \tanh\left(\frac{1}{2}\sqrt{\frac{2b + c^2\alpha + a^2\beta - 3(2b + c^2\alpha + a^2\beta)}{\epsilon^2(\beta + \alpha\mu^2)}}\,\xi\right)\right) \frac{ie^{i(-ct+ax+by)}\,\epsilon^2\sqrt{\beta + \alpha\mu^2}\sqrt{\frac{2b+c^2\alpha+a^2\beta-3(2b+c^2\alpha+a^2\beta)}{\epsilon^2(\beta+\alpha\mu^2)m_4}}\sqrt{m_4}}{2\sqrt{\gamma}} + \frac{\sqrt{2b + c^2\alpha + a^2\beta}}{\sqrt{2}\sqrt{\gamma}}. \tag{5.17}$$

6. Graphical results and discussions

The visual representations of the DTDP equation are investigated in this section. The DTDP equation can be represented visually by the use of the IMETFM with multiple parametric predictions leading to diverse soliton solutions. The framework of DTDP equation stated in Eq (2.1) is analyzed by varying parameter constraints. By modifying the settings of the parameters, visualizations of the DTDP equation can be altered. In addition to contour visualizations, 3D and 2D illustrations are also provided for ease of understanding. Solitary waves are created by employing the aforementioned techniques in various patterns including kink, bell-shaped, singular wave, periodic, singular periodic wave, bright and dark solitary wave, breather, singular bell, M-shaped, W-shaped, and V-pattern types of solitons. Changes in the value of the parameter leads to a small modification of the solitary wave without modifying its curve shape. Figure 1 shows $|\Psi_1(x, y, t)|$ for the solution of Eq (5.3) obtained by concentrating on the parametric elements $\epsilon = 1$, $\beta = 2$, $y = 0$, $\gamma = 2$, $a = 2$, $c = 1$, $b = 1$, $\mu = 2$, and $\alpha = 2$, which produces a bell-shaped soliton. Figure 2 shows $\mathrm{Re}[\Psi_2(x, y, t)]$ for the solution of Eq (5.4) obtained by concentrating on the parametric elements $\epsilon = 1$, $\beta = 2$, $y = 0$, $\gamma = -2$, $a = 2$, $c = -0.1$, $b = -0.1$, $\mu = 2$, and $\alpha = 2$, which produces a breather soliton. Figure 3 exemplifies $|\Psi_3(x, y, t)|$ for the solution of Eq (5.5) obtained by concentrating on the parametric elements $\epsilon = -1$, $\beta = 2$, $y = 0$, $\gamma = 1$, $a = 1$, $c = 1$, $b = 1$, $\mu = 2$, and $\alpha = 1$, which provides a singular bell pattern. Figure 4 represents $|\Psi_4(x, y, t)|$ for the solution of Eq (5.6) obtained by concentrating on the parametric elements $\epsilon = 1$, $\beta = 1$, $y = 0$, $\gamma = 2$, $a = 1$, $c = 2$, $\mu = 1$, and $\alpha = 1$, which provides a singular periodic wave. Figure 5 shows $|\Psi_5(x, y, t)|$ for the solution of Eq (5.7) obtained by concentrating on the parametric elements $\epsilon = -1$, $\beta = -4$, $y = 0$, $\gamma = 1$, $a = 2$, $c = 2$, $b = 1$, $\mu = 2.5$, and $\alpha = 2.7$, which provides a V-pattern soliton. Figure 6 displays $|\Psi_6(x, y, t)|$ for the solution of Eq (5.8) obtained by concentrating on the parametric elements $\epsilon = 1$, $\beta = 2$, $y = 0$, $\gamma = 1$, $a = 1$, $c = 1$, $b = 1$, $\mu = 1$, $\alpha = 0.1$, and $n = -0.4$, which provides a periodic wave soliton. Figure 7 shows $\mathrm{Im}[\Psi_{10}(x, y, t)]$ for the solution of Eq (5.12) obtained by concentrating on the parametric elements $\epsilon = 1$, $\beta = 2$, $y = 0$, $\gamma = 1$, $b = 1$, $a = 0$, $\alpha = -0.2$, $c = 0.4$, $\mu = 0.2$, $m_4 = -2$, and $m_3 = 2$, which provides bright and dark soliton. Figure 8 presents $|\Psi_{11}(x, y, t)|$ for the solution of Eq (5.13) obtained by concentrating on the parametric elements $\epsilon = 1$, $\beta = 3$, $y = 0$, $\gamma = 1$, $b = 0$, $a = 1$, $\alpha = -0.2$, $c = 0.1$, $\mu = -0.1$, $m_4 = -3$, and $m_3 = 0.01$, which provides a W-pattern soliton. Figure 9 displays $\mathrm{Re}[\Psi_{13}(x, y, t)]$ for

the solution of Eq (5.15) obtained by concentrating on the parametric elements $\epsilon = -1, \beta = 0, y = 0, \gamma = 0.2, m_0 = 0.001, \alpha = 0.01, \mu = 0.2, c = -0.1, b = 0$, and $a = -0.1$, which provides a singular wave soliton. Figure 10 displays $|\Psi_{14}(x, y, t)|$ for the solution of Eq (5.16) obtained by concentrating on the parametric elements $\epsilon = 1, \beta = 2, y = 0, \gamma = 0.2, \alpha = 0.01, \mu = 0.2, c = -0.1, b = 1.2, a = -0.1$, and $m_1 = 1$, which provides a M-pattern soliton. Figure 11 presents $\mathrm{Re}[\Psi_{15}(x, y, t)]$ for the solution of Eq (5.17) obtained by concentrating on the parametric elements $\epsilon = 1, \beta = -0.9, y = 0, \gamma = 2, \alpha = 2, \mu = 0.06, c = 0.01, b = 5, a = 0, m_2 = 4$, and $m_4 = 1$, which provides a kink shape soliton.

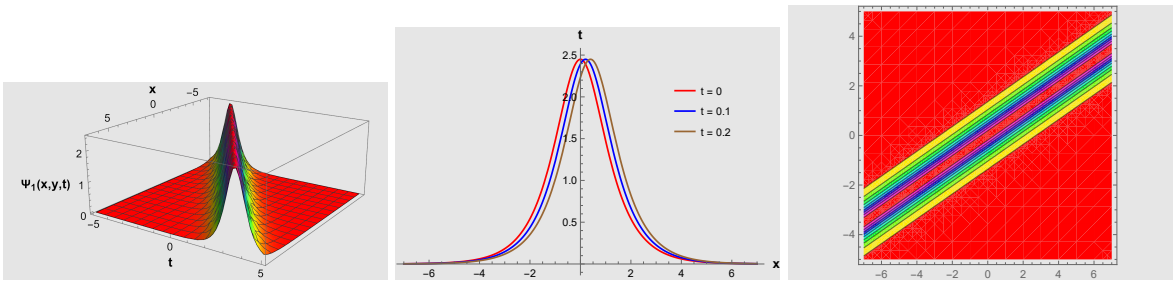

(a) 3D Plot (b) 2D Plot (c) Contour Plot

Figure 1. The 3D, 2D, and contour plots of a bell-shaped soliton solution $|\Psi_1(x, y, t)|$ given in Eq (5.3) at various time intervals using different values of the parameters $\epsilon = 1, \beta = 2, y = 0, \gamma = 2, a = 2, c = 1, b = 1, \mu = 2$, and $\alpha = 2$: (a) 3D space-time graph, (b) 2D graph, and (c) contour plot.

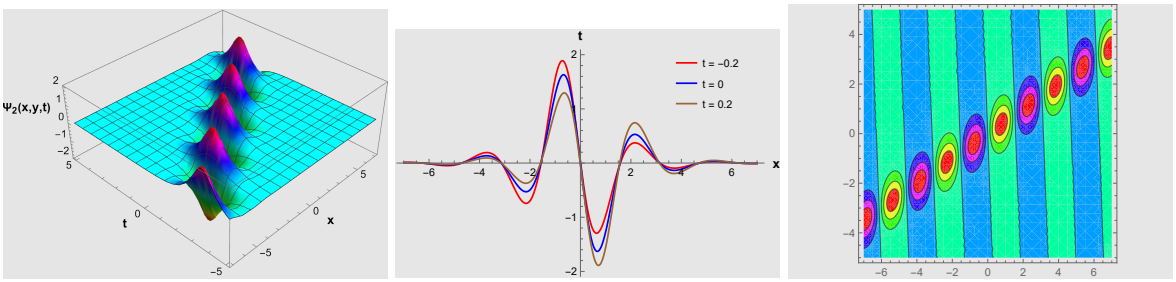

(a) 3D Plot (b) 2D Plot (c) Contour Plot

Figure 2. The 3D, 2D, and contour plots of a breather soliton solution $\mathrm{Re}[\Psi_2(x, y, t)]$ given in Eq (5.4) at various time intervals using different values of the parameters $\epsilon = 1, \beta = 2, y = 0, \gamma = -2, a = 2, c = -0.1, b = -0.1, \mu = 2$, and $\alpha = 2$: (a) 3D plot, (b) 2D graph, and (c) contour graph.

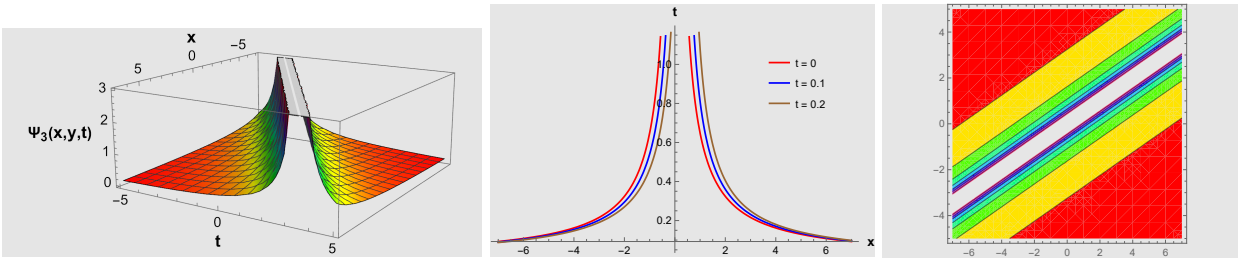

(a) 3D Plot (b) 2D Plot (c) Contour Plot

Figure 3. The 3D, 2D, and contour plots of a singular bell pattern solution $|\Psi_3(x, y, t)|$ given in Eq (5.5) at various time intervals using different values of the parameters $\epsilon = -1$, $\beta = 2$, $y = 0$, $\gamma = 1$, $a = 1$, $c = 1$, $b = 1$, $\mu = 2$, and $\alpha = 1$: (a) 3D profile plot, (b) 2D graph, and (c) contour graph.

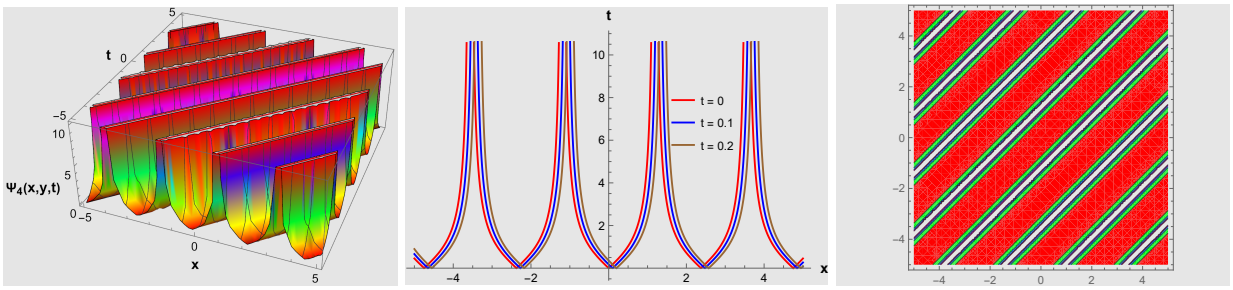

(a) 3D Plot (b) 2D Plot (c) Contour Plot

Figure 4. The 3D, 2D, and contour graphs of a singular periodic solution $|\Psi_4(x, y, t)|$ given in Eq (5.6) at various time ranges using different values of the parameters $\epsilon = 1$, $\beta = 1$, $y = 0$, $\gamma = 2$, $a = 1$, $c = 2$, $\mu = 1$, and $\alpha = 1$: (a) 3D space-time map, (b) 2D plot, and (c) contour graph.

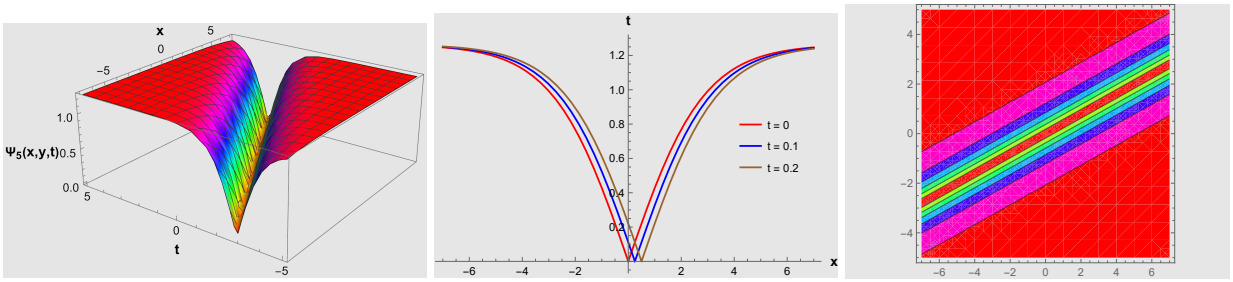

(a) 3D Plot (b) 2D Plot (c) Contour Plot

Figure 5. The 3D, 2D, and contour graphs of a V-pattern solution $|\Psi_5(x, y, t)|$ given in Eq (5.7) at many time levels using different values of the parameters $\epsilon = -1$, $\beta = -4$, $y = 0$, $\gamma = 1$, $a = 2$, $c = 2$, $b = 1$, $\mu = 2.5$ and $\alpha = 2.7$: (a) 3D profile plot, (b) 2D graph and (c) contour graph.

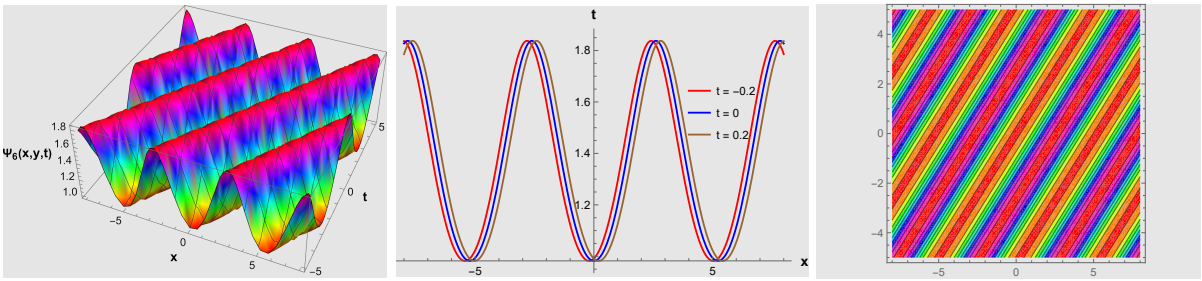

(a) 3D Plot (b) 2D Plot (c) Contour Plot

Figure 6. The 3D, 2D, and contour graphs of a periodic wave solution $|\Psi_6(x, y, t)|$ given in Eq (5.8) at various time ranges using different values of the parameters $\epsilon = 1, \beta = 2, y = 0, \gamma = 1, a = 1, c = 1, b = 1, \mu = 1, \alpha = 0.1$, and $n = -0.4$: (a) 3D space-time map, (b) 2D graph, and (c) contour plot.

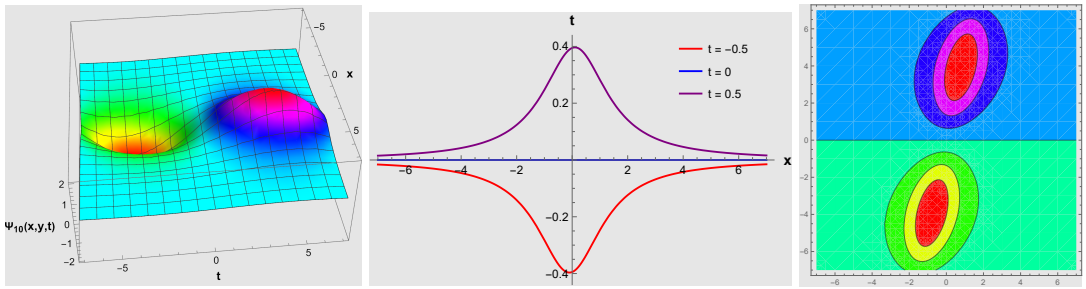

(a) 3D Plot (b) 2D Plot (c) Contour Plot

Figure 7. The 3D, 2D, and contour graphs of a bright and dark soliton solution $\mathrm{Im}[\Psi_{10}(x, y, t)]$ given in Eq (5.12) at various time interval using different values of the parameters $\epsilon = 1, \beta = 2, y = 0, \gamma = 1, b = 1, a = 0, \alpha = -0.2, c = 0.4, \mu = 0.2$, $m_4 = -2$, and $m_3 = 2$: (a) 3D space-time plot, (b) 2D graph, and (c) contour graph.

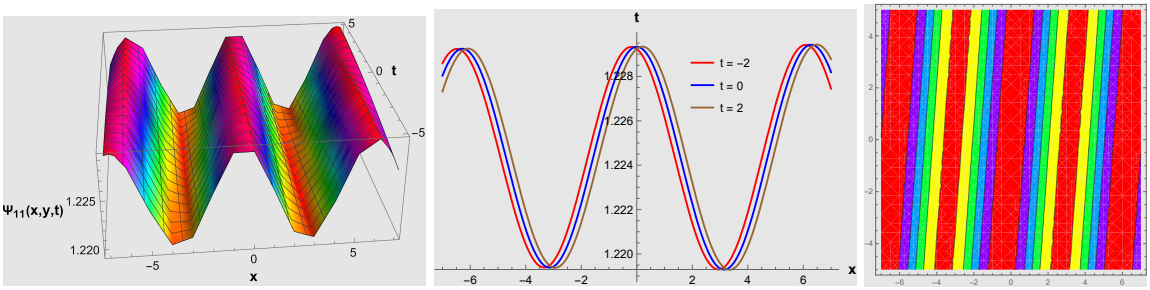

(a) 3D Plot (b) 2D Plot (c) Contour Plot

Figure 8. The 3D, 2D, and contour graphs of a W-pattern soliton solution $|\Psi_{11}(x, y, t)|$ given in Eq (5.13) at unique time levels using different values of the parameters $\epsilon = 1, \beta = 3, y = 0, \gamma = 1, b = 0, a = 1, \alpha = -0.2, c = 0.1, \mu = -0.1, m_4 = -3$, and $m_3 = 0.01$: (a) 3D plot, (b) 2D profile graph, and (c) contour map.

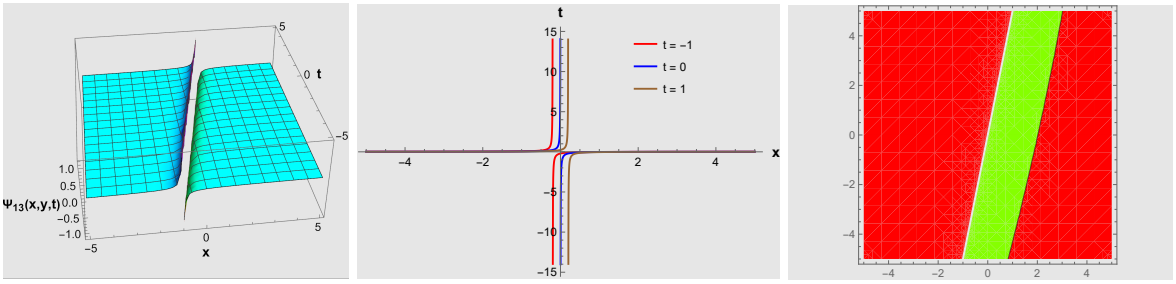

(a) 3D Plot (b) 2D Plot (c) Contour Plot

Figure 9. The 3D, 2D, and contour plots of a singular wave solution $\mathrm{Re}[\Psi_{13}(x, y, t)]$ given in Eq (5.15) at novel time intervals using different values of the parameters $\epsilon = -1$, $\beta = 0$, $y = 0$, $\gamma = 0.2$, $m_0 = 0.001$, $\alpha = 0.01$, $\mu = 0.2$, $c = -0.1$, $b = 0$, and $a = -0.1$: (a) 3D space-time visualization, (b) 2D graph, and (c) contour profile plots.

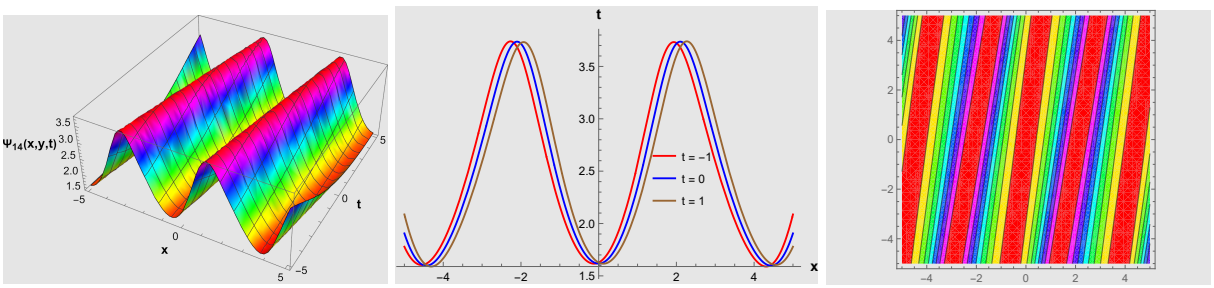

(a) 3D Plot (b) 2D Plot (c) Contour Plot

Figure 10. The 3D, 2D, and contour graphs of a M-pattern soliton solution $|\Psi_{14}(x, y, t)|$ given in Eq (5.16) at various time intervals using different values of the parameters $\epsilon = 1$, $\beta = 2$, $y = 0$, $\gamma = 0.2$, $\alpha = 0.01$, $\mu = 0.2$, $c = -0.1$, $b = 1.2$, $a = -0.1$, and $m_1 = 1$: (a) 3D space-time plot, (b) 2D graph, and (c) contour visualization.

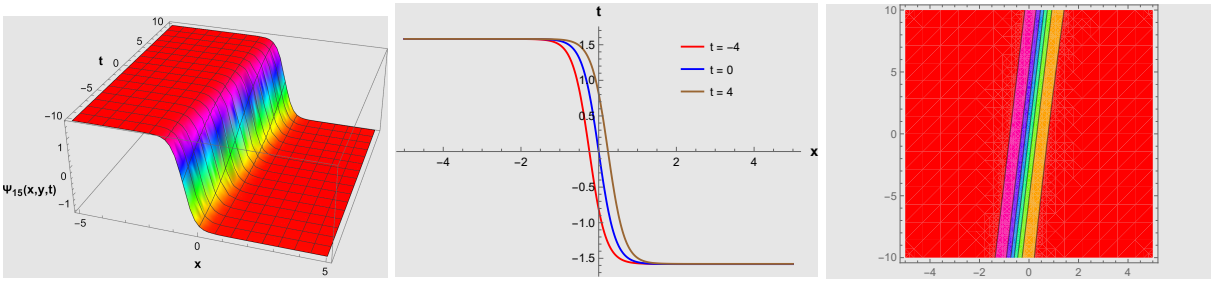

(a) 3D Plot (b) 2D Plot (c) Contour Plot

Figure 11. The 3D, 2D, and contour graphs of a kink wave solution $\mathrm{Re}[\Psi_{15}(x, y, t)]$ given in Eq (5.17) at different time ranges using different values of the parameters $\epsilon = 1$, $\beta = -0.9$, $y = 0$, $\gamma = 2$, $\alpha = 2$, $\mu = 0.06$, $c = 0.01$, $b = 5$, $a = 0$, $m_2 = 4$, and $m_4 = 1$: (a) 3D profile visualization, (b) 2D graph, and (c) contour plot.

7. Bifurcation analysis

Bifurcation analysis of the DTDP equation shows how variations in the parameters affect the dynamical structure of the system. Utilizing the planar dynamical system methods, bifurcation points at which the system becomes unstable, changing from a stable one, are identified. Using Eq (2.1), the dynamic planner system can be represented as:

$$\begin{cases} \frac{dZ}{d\xi} = P, \\ \frac{dP}{d\xi} = \sigma_1 Z - \sigma_2 Z^3, \end{cases} \tag{7.1}$$

with Hamiltonian function is given by,

$$H(Z,P) = \frac{P^2}{2} - \sigma_1 \frac{Z^2}{2} + \sigma_2 \frac{Z^4}{4} = h, \tag{7.2}$$

where,

$$\sigma_1 = \frac{2b + c^2\alpha + a^2\beta}{\mu^2\alpha + \beta}, \quad \sigma_2 = \frac{2\gamma}{\mu^2\alpha + \beta},$$

and the Hamiltonian constant is denoted by h. The system (7.1) has three equilibrium points,

$$M_1 = (0,0), \quad M_2 = \sqrt{\frac{\sigma_1}{\sigma_2}}, \quad M_3 = -\sqrt{\frac{\sigma_1}{\sigma_2}}.$$

For Eq (7.1) the Jacobian is,

$$J(Z,P) = \begin{vmatrix} 0 & 1 \\ \sigma_1 - 2\sigma_2 Z^3 & 0 \end{vmatrix} = 2\sigma_2 Z^3 - \sigma_1 \ .$$

For an equilibrium point M of a Hamiltonian system, three cases can be examined: If $(J)_M = 0$, then M is a cuspid; if $(J)_M < 0$, then M is a saddle; if $(J)_M > 0$, then M is a center. Thus, the bifurcation behavior for the system (7.1) can be characterized as shown below:

Case 1: If $\sigma_1 > 0, \sigma_2 > 0$, then $\alpha = 2, \beta = -1, \gamma = -\frac{1}{2}, b = -1, a = 1, c = 1, \mu = 0$ gives $M_1 = (0,0)$, $M_2 = (1,0)$, $M_3 = (-1,0)$, and M_1 is serves as a saddle point, while the M_2 and M_3 are center points as shown in Figure 12.

Case 2: If $\sigma_1 < 0, \sigma_2 < 0$, then $\alpha = -2, \beta = -1, \gamma = \frac{1}{2}, b = 2, a = 1, c = 1, \mu = 0$ gives $M_1 = (0,0)$, $M_2 = (1,0)$, $M_3 = (-1,0)$, and M_1 is clearly center point, while the M_2 and M_3 are saddle points as shown in Figure 13.

Case 3: If $\sigma_1 < 0, \sigma_2 > 0$, then $\alpha = -4, \beta = -1, \gamma = \frac{1}{2}, b = 2, a = 1, c = 1, \mu = 0$ gives $M_1 = (0,0)$, $M_2 = (i,0)$, $M_3 = (-i,0)$, and M_1 is represented as saddle point,but M_2 and M_3 are center points.

Case 4: If $\sigma_1 > 0, \sigma_2 < 0$, then $\alpha = -2, \beta = -1, \gamma = -\frac{1}{2}, b = 2, a = 1, c = 1, \mu = 0$ gives $M_1 = (0,0)$, $M_2 = (i,0)$, $M_3 = (-i,0)$, and M_1 is clearly a center point, whereas the M_2 and M_3 are saddle points.

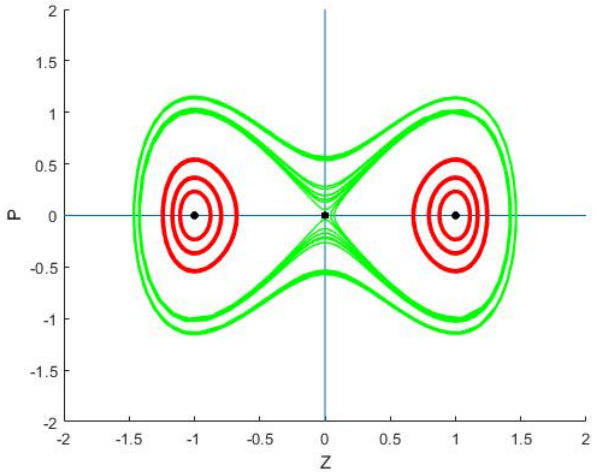

Figure 12. $\sigma_1 > 0, \sigma_2 > 0$.

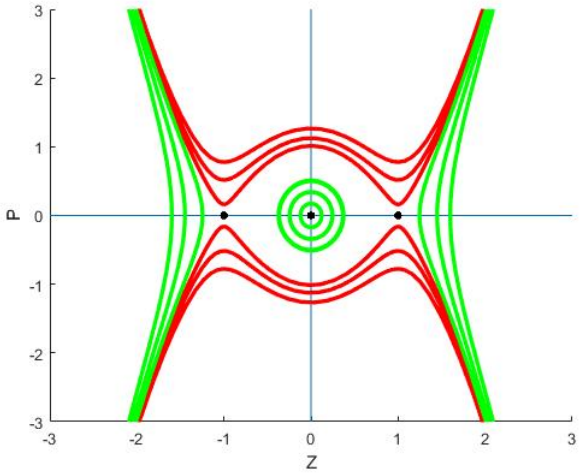

Figure 13. $\sigma_1 < 0, \sigma_2 < 0$.

8. Chaotic behaviours

The study of chaotic behavior extends our understanding of the complexity of the paraxial system. Analytical observations show that the system displays irregular but deterministic dynamics in some regimes of parameters. This chaotic development is a demonstration of the sensitive dependence of nonlinear systems on the initial conditions, and parameter values and serves to supplement the bifurcation analysis by demonstrating how instabilities increase to form complex motion. This section examines the presence of chaotic behavior in the resulting system (7.1) by adding a perturbed term. The discussion involves 2D, time series, and 3D phase portraits for the system. The following dynamical

system is investigated:

$$\begin{cases} \frac{dZ}{d\xi} = P, \\ \frac{dP}{d\xi} = \sigma_1 Z - \sigma_2 Z^3 + \delta \cos(\nu\xi), \end{cases} \tag{8.1}$$

where $\delta \cos(\nu\xi)$ is used to represent perturbation, with δ referring to the magnitude and ν referring to frequency of the system. This part analyzes the effect of the perturbation's intensity and frequency on Eq (8.1). With the main parameters set as $\alpha = 2$, $\beta = -1$, $\gamma = -\frac{1}{2}$, $b = -1$, $a = 1$, $c = 1$, and $\mu = 0$, periodic, quasi periodic, and chaotic behavior appear for various perturbation intensities and frequencies, as shown in Figures 14–16. Figure 14 shows the response of Eq (8.1) when ($\delta = 0.1$, $\nu = 0.2$) demonstrating variations in the trajectory as a function of the perturbation's strength and frequency. Periodicity in Eq (8.1) is illustrated by way of time series, 2D, and 3D phase plots. Outcomes in Figure 15 are shown to transit from periodic to quasi periodic behavior upon a slight increase in strength and frequency ($\delta = 4$, $\nu = 2\pi$). In Figure 16, a further increase in frequency (δ increases to $\delta = 2$, $\nu = \pi$) triggers high perturbations, driving the system to chaotic conditions.

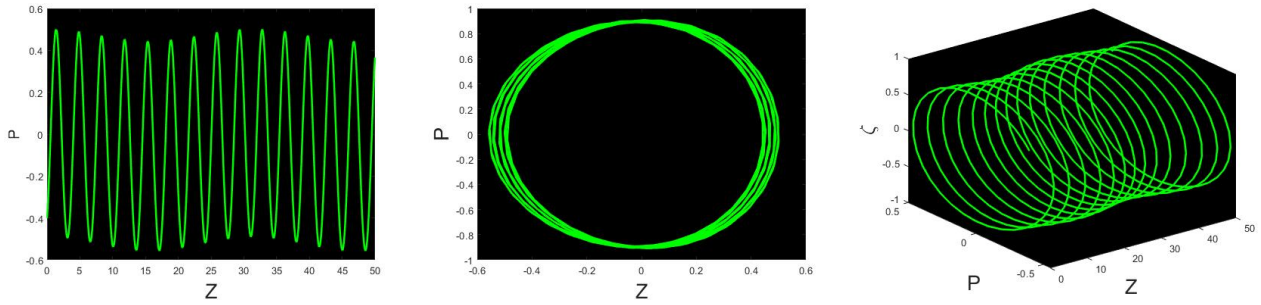

(a) Time Series (b) 2D Plot (c) 3D Plot

Figure 14. Chaotic behaviour at $\delta = 0.1$ and $\nu = 0.2$.

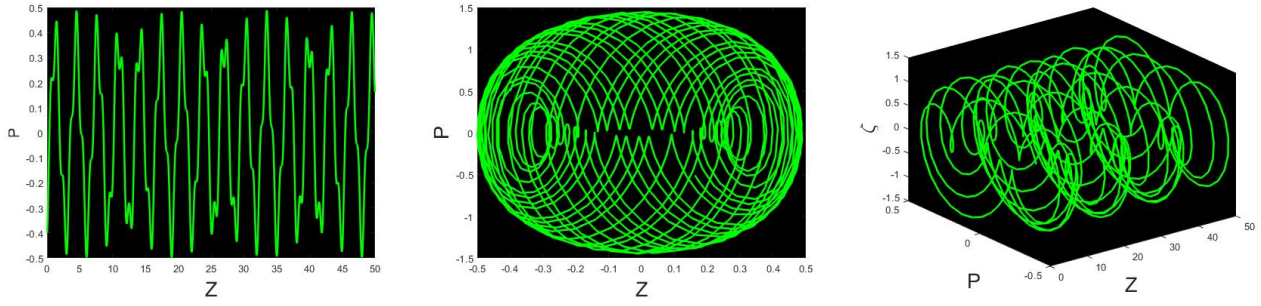

(a) Time Series (b) 2D Plot (c) 3D Plot

Figure 15. Chaotic behaviour at $\delta = 4$ and $\nu = 2\pi$.

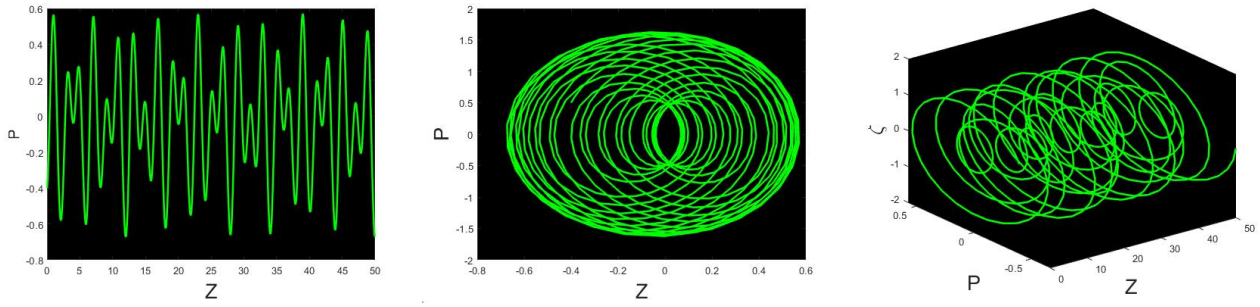

(a) Time Series (b) 2D Plot (c) 3D Plot

Figure 16. Chaotic behaviour at $\delta = 2$ and $\nu = \pi$.

9. Sensitivity analysis

The sensitivity analysis reveals how the solutions of the DPDP equation react to small changes in the initial conditions and the system's parameters. The findings show that even minimal changes can modify the evolution of the solitary wave profiles, influencing their stability and long-term behavior. Sensitivity analysis gives better insight into the robustness of the soliton solutions obtained and determines under what conditions the waveforms preserve their structure or diverge into other dynamical patterns. This section gives the sensitivity analysis of the dynamical system (7.1) for the parameters $\alpha = 2, \beta = -1, \gamma = -\frac{1}{2}, b = -1, a = 1, c = 1$, and $\mu = 0$. The system's initial conditions are as follows,

(1) $(Z, P) = (0.9, 0.2)$ for the red curve and $(Z, P) = (0.9, 0.5)$ for the blue curve,
(2) $(Z, P) = (0.9, 0.3)$ for the red curve and $(Z, P) = (0.9, 0.7)$ for the green curve,
(3) $(Z, P) = (0.9, 0.5)$ for the blue curve and $(Z, P) = (1.6, 1.6)$ for the green curve,
(4) $(Z, P) = (0.5, 0.2)$ for the red curve , $(Z, P) = (0.9, 0.5)$ for the blue curve, and $(Z, P) = (1.6, 1.6)$ for the green curve.

The findings yielded by this successful scheme are shown in Figures 17–20.

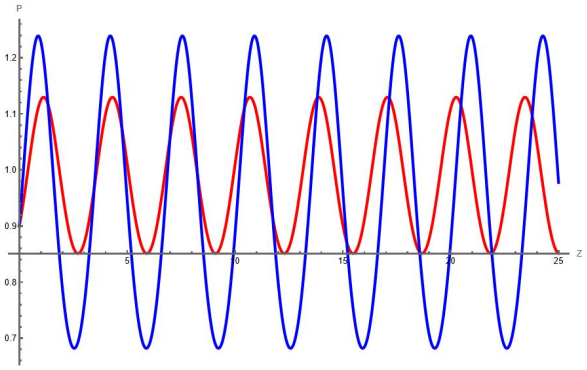

Figure 17. Sensitivity analysis of the Eq (7.1) for the initial points $(Z, P) = (0.9, 0.2)$ for the red curve and $(Z, P) = (0.9, 0.5)$ for the blue curve.

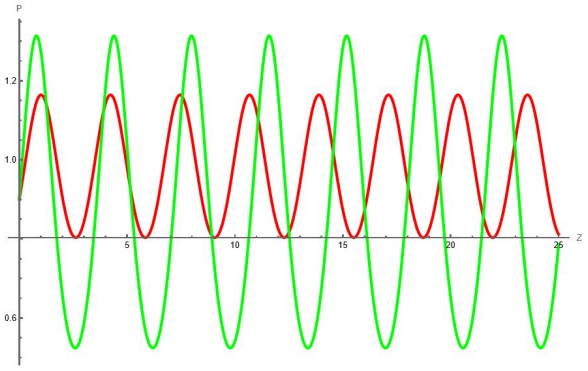

Figure 18. Sensitivity analysis of the Eq (7.1) for the initial points $(Z, P) = (0.9, 0.3)$ for the red curve and $(Z, P) = (0.9, 0.7)$ for the green curve.

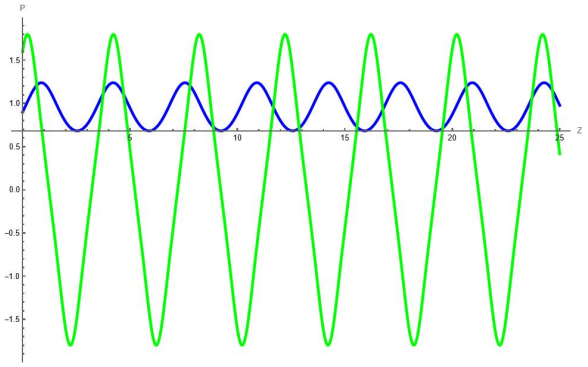

Figure 19. Sensitivity analysis of the Eq (7.1) for the initial points $(Z, P) = (0.9, 0.5)$ for the blue curve and $(Z, P) = (1.6, 1.6)$ for the green curve for the green curve.

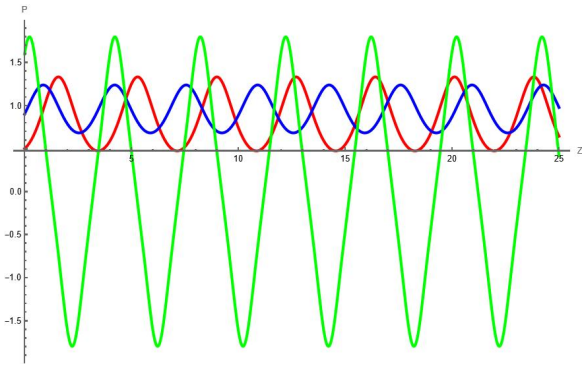

Figure 20. Sensitivity analysis of the Eq (7.1) for the initial points $(Z, P) = (0.5, 0.2)$ for the red curve, $(Z, P) = (0.9, 0.5)$ for the blue curve, and $(Z, P) = (1.6, 1.6)$ for the green curve.

10. Physical interpretation

The DTDP equation was created in the 1970s by scientists working mainly in wave theory and nonlinear optics. It was based on work by scientists such as Zakharov and Shabat, who researched solitons and the evolution of wave packets. It developed from scaling the nonlinear Schrödinger equation into a dimensionless equation to make it easier. The equation describes the balance of diffraction, dispersion, and nonlinearity in media. Its establishment enabled an understanding of phenomena in optics, Bose–Einstein condensates, and fluid dynamics.

- $i\Psi_y$ refers to the evolution of the wave envelope Ψ along the y-axis. In physical systems, y can be used for the propagation distance, such as in optics, where light propagates through a fiber or a medium.
- $\frac{\alpha}{2}\Psi_{tt}$ is temporal dispersion, similar to how a wave disperses or compresses with time. If $\alpha > 0$, the pulse will spread out (normal dispersion) but if $\alpha < 0$, it can compress or focus (anomalous dispersion).
- $\frac{\beta}{2}\Psi_{xx}$ is the spatial diffraction term, telling us how the wave spreads out or curves in the transverse spatial direction x. It is similar to how a laser beam slowly spreads as it travels through space.
- $\gamma|\Psi|^2\Psi$ is a nonlinear term that simulates self-interaction depending on the wave's intensity. When $\gamma > 0$, the wave focuses itself (resulting in bright solitons) but when $\gamma < 0$, it becomes defocusing (leading to dark solitons).

By applying the IMETFM technique to the DTDP equation, a broad range of solitary wave solutions with different shapes and their respective physical interpretations can be found.

- Kink solutions are abrupt, localized jumps from one state to another, typically understood as domain walls or phase boundaries in magnetic materials and nonlinear optical media.
- Bell-shaped solitary waves have smooth, localized hump-like shapes that bear packages of energy that will preserve their profiles as they travel. Examples include non-dispersive wave pulses such as optical solitons or surface water waves.
- Singular wave solutions exhibit points of infinite amplitude or discontinuity, usually representing physical effects such as filamentation in lasers or the triggering of blow-up behaviors in nonlinear media.
- Periodic solutions recur periodically in time or in space, embodying stable wave trains or patterns like crystal lattices or photonic arrays.
- Periodic singular solutions blend periodicity and singularities localized at one point, capturing phenomena where periodic wave dynamics are interrupted by sharp spike-like intensities, applicable in plasma dynamics or nonlinear optics.
- Bright solitary waves are locally intensified pulses with greater intensity than the ambient, characteristic in attractive nonlinear media where the energy is concentrated in robust wave packets.
- Dark solitary waves manifest as a local depression of a continuous wave background, occurring in defocusing media like optical fibers with repulsive nonlinearities or Bose–Einstein condensates with intensity or density notches.
- Breather solitons are spatially and temporally oscillating localized solutions that represent pulsating energy packets or modulation instabilities in nonlinear lattices and optical fibers.

- Singular bell-shaped waves are localized hump structures embedded with singularities, exhibiting extreme nonlinear events like sudden energy concentrations or rogue waves.
- The physical realization of a V-pattern soliton usually corresponds to its appearance as a wave structure showing two sloping wave fronts intersecting to create a characteristic V-shape. This is often seen in nonlinear dispersive systems when solitons interact or travel with angular components.

Moreover, physical description of these solutions in concise form can be shown in Table 1. Together, this rich, multifaceted family of solutions represents the complexity and diversity of wave phenomena under the paraxial equation. They facilitate further insight into many physical processes like energy localization, wave switching, pulse interactions, pattern formation, and nonlinear instabilities, hence yielding insightful information regarding the behavior and control of nonlinear waves in numerous scientific and engineering disciplines.

Table 1. Solitary wave solutions and their physical interpretations.

Solution type	Shape	Physical meaning
Kink	Step-like	Domain wall, phase transition boundary
Bell-shaped	Single hump	Optical soliton, water wave packet
Singular	Blow-up point	Filamentation, loss of regularity
Periodic	Regular repetition	Wave trains, crystal lattices
Singular periodic	Spiked repetition	Shock trains, periodic energy blow-up
Bright soliton	Localized peak	Light pulse in a fiber, or a matter-wave soliton
Dark soliton	Localized dip	Intensity drop in a laser beam, density dip in Bose–Einstein condensates
Breather	Localized, oscillating	Pulsating light, envelope soliton
Singular bell	Hump with a singularity	Extreme events in nonlinear media
M-shaped	Double hump	Twin pulse propagation
W-shaped	Triple hump	Multi-pulse interaction
V-pattern	Stable localized wave packets	Interaction of obliquely propagating wave fronts, forming a V-shaped stable wave structure due to nonlinear dispersive balance

11. Comparison, advantages, and limitations

The IMETFM is a sophisticated mathematical method employed to identify exact traveling wave solutions of complex NLPDEs. It surpasses standard tanh-function methods because it supports the derivation of more diverse types of wave solutions for intricate nonlinear systems. The comparison of IMETFM with classical tanh method is shown in Table 2.

11.1. Advantages

It effectively derives new and varied exact solutions such as bright solitons, dark solitons, bright–dark solitons, single solitons, multiple solitons, periodic solutions, singular periodic solutions, hyperbolic, rational, trigonometric, and exponential function solutions. It is capable of dealing with

complicated NLPDEs, such as fractional and high-dimensional equations, by transforming them into conventional ODEs through wave transformations. The technique relies on a powerful algebraic scheme that systematically connects coefficients and parameters to form solutions. It can be used both for integrable and non-integrable equations, increasing its applicability. The procedure is aided by symbolic computational tools, making it easy to apply and verify.

11.2. Limitations

As with many analytical techniques, it can involve complex algebraic manipulations and symbolic computation, which may be computationally intensive for extremely complicated equations. The usefulness of the procedure relies on the possibility of reducing PDEs to ODEs through wave transformations, which may not always be simple. Others can be hard to visualize physically or need further analysis to establish whether they have any relevance to particular physical problems. It might not be generally applicable to all nonlinear PDEs, particularly those with missing some mathematical structures compatible with the tanh-function method.

Table 2. Comparison analysis.

Aspect	Classical tanh method	IMETFM
Basic idea	Uses hyperbolic tangent function to find traveling wave solutions of nonlinear PDEs	Extends the classical method with more flexible ansatz forms and coefficient schemes for wider solution types
Solution types	Finds exact traveling wave solutions, mainly simple solitons and periodic waves	Generates a broader spectrum including bright/dark solitons, breathers, rational, and periodic solutions
Complexity and scope	Limited to simpler nonlinear evolution and wave equations	Suitable for more complex nonlinear differential equations with richer wave structures
Analytical procedure	Reduces PDEs to ODEs then assumes the solution in tanh form	Uses extended solution forms and coefficient comparison yielding diverse exact solutions
Application flexibility	Effective for many standard nonlinear wave models	More powerful for complex/extended nonlinear models requiring varied wave structures
Stability and sensitivity analysis	Typically not included in basic methods	Often integrated with stability and bifurcation analysis for deeper dynamical insights

12. Stability

This section will look at the stability analysis for regulating Eq (2.1). Linear and nonlinear stability methods are used to examine the system's behavior. Stability conditions are established through perturbation methods. Let us the form's perturbed solution,

$$\Psi(x, y, t) = b_0 A(x, y, t) + b_1. \tag{12.1}$$

Any constant b_1 is a steady-state solution for Eq (2.1), as is readily apparent. Equation (12.1) can be entered into Eq (2.1) to produce,

$$\gamma A^3 b_0^3 + 3\gamma A^2 b_0^2 b_1 + 3\gamma A b_0 b_1^2 + \gamma b_1^3 + \frac{1}{2}\alpha b_0 A_{tt} + i b_0 A_y + \frac{1}{2}\beta b_0 A_{xx} = 0.$$

The equation above is linearized in b_0,

$$3\gamma A b_0 b_1^2 + \frac{1}{2}\alpha b_0 A_{tt} + i b_0 A_y + \frac{1}{2}\beta b_0 A_{xx} = 0. \tag{12.2}$$

Now we take the solution of Eq (12.2) in the form,

$$A(x, y, t) = e^{i(lx+my+nt)}. \tag{12.3}$$

Now, taking the derivatives of equation above, then the following equation is obtained by putting these derivatives in Eq (12.2).

$$b_0\left(2m + n^2\alpha + l^2\beta - 6\gamma b_1^2\right) = 0. \tag{12.4}$$

Solving Eq (12.4) for l, we have

$$l = \frac{\sqrt{-2m - n^2\alpha + 6\gamma b_1^2}}{\sqrt{\beta}}.$$

Clearly from $l > 0$ and Figure 21, the system (2.1) is stable.

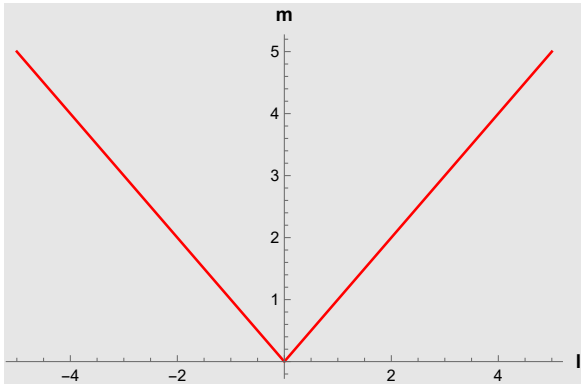

Figure 21. Stability analysis graph.

The nonlinear stability concept extends beyond the boundaries of linear stability analysis in the sense that it takes the influence of nonlinear disturbances upon the system's behavior into account.

In this formulation, small deviations in the system's parameters or the initial conditions cause large deviations in the wave trajectories, indicating the system's sensitivity to nonlinear effects. This sensitivity appears as chaos, as demonstrated in Figure 16, where the solutions have irregular but bounded oscillations. These chaotic dynamics emphasize that even when the solutions look stable in linear analysis, they can still get destabilized by the interaction of nonlinearities. The incorporation of chaotic motion thus offers a more profound and realistic insight into the nonlinear stability of the derived solutions.

13. Conclusions

In this research, the application of the IMETFM to the DTDP equation has yielded a rich variety of solitary wave solutions. Diverse soliton solutions like kink, bell-shaped, singular wave, periodic, singular periodic wave, bright and dark solitary wave, breather soliton, singular bell, M-shaped, W-shaped, and V-pattern solitons are obtained. These solutions are graphically depicted by vivid 2D and 3D graphical presentations, which expose the intricate soliton structures and wave interactions. Contour plots also offer effective visualizations of the wave profiles and spatial behaviors, revealing the complex dynamics of the equation. The simultaneous application of 2D, 3D, and contour analyses not only confirms the results of the analysis but also deepens our insight into multi-dimensional nonlinear wave phenomena described by the DTDP equation. Bifurcation, chaotic, and sensitivity analyses of the system also discussed. The complete methodology shows the robustness of the IMETFM in investigating rich solution patterns in higher-dimensional NLPDEs.

Author contributions

Arooma Zainab: Methodology, investigation, writing–original draft; Muhammad Abbas: Supervision, writing–original draft, writing–review and editing; Yagoub A. S. Arko: Software, investigation, writing–review and editing; Alina Alb Lupas: Formal analysis, investigation, writing–review and editing; Tahir Nazir: Supervision, writing–original draft, writing–review and editing; Muhammad Zain Yousaf: Formal analysis, investigation, writing–review and editing. All authors have read and approved the final version of the manuscript for publication.

Use of Generative AI tools declaration

The authors declare they have not used artificial intelligence (AI) tools in the creation of this article.

Acknowledgments

The authors would like to acknowledge the Deanship of Graduate Studies and Scientific Research, Taif University for funding this work. The publication of this research was supported by the University of Oradea, Romania.

Conflict of interest

There is no conflict of interest.

References

1. J. R. M. Borhan, M. Mamun Miah, F. Z. Duraihem, M. A. Iqbal, W. X. Ma, New optical soliton structures, bifurcation properties, chaotic phenomena, and sensitivity analysis of two nonlinear partial differential equations, *Int. J. Theor. Phys*., **63** (2024), 183. https://doi.org/10.1007/s10773-024-05713-9
2. A. Farooq, T. Shafique, M. Abbas, A. Birhanu, Y. S. Hamed, Explicit travelling wave solutions to the time fractional Phi-four equation and their applications in mathematical physics, *Sci. Rep.*, **15** (2025), 1683. https://doi.org/10.1038/s41598-025-86177-7
3. G. Zhang, W. Weng, Z. Yan, On large-space and long-time asymptotic behaviors of kink-soliton gases in the sine-Gordon equation, *arXiv*, 2025, arXiv:2501.03493. https://doi.org/10.48550/arXiv.2501.03493
4. M. Vivas-Cortez, M. Nageen, M. Abbas, M. Alosaimi, Investigation of analytical soliton solutions to the non-linear Klein-Gordon model using efficient techniques, *Symmetry*, **16** (2024), 1085. https://doi.org/10.3390/sym16081085
5. K. U. Tariq, J. G. Liu, S. Nisar, Study of explicit travelling wave solutions of nonlinear (2+1)-dimensional Zoomeron model in mathematical physics, *J. Nonlinear Complex Data Sci.*, **25** (2024), 109–124. https://doi.org/10.1515/jncds-2023-0068
6. S. Arshed, G. Akram, M. Sadaf, M. Irfan, M. Inc, Extraction of exact soliton solutions of (2+1)-dimensional Chaffee-Infante equation using two exact integration techniques, *Opt. Quantum Electron.*, **56** (2024), 988. https://doi.org/10.1007/s11082-024-06470-z
7. A. A. Mamun, C. Lu, S. N. Ananna, M. M. Uddin, Rational sine-Gordon expansion method to analyze the dynamical behavior of the time-fractional phi-four and (2+1)-dimensional CBS equations, *Sci. Rep.*, **14** (2024), 9473. https://doi.org/10.1038/s41598-024-60156-w
8. P. R. Kundu, M. R. A. Fahim, M. E. Islam, M. A. Akbar, The sine-Gordon expansion method for higher-dimensional NLEEs and parametric analysis, *Heliyon*, **7** (2021), e06459. https://doi.org/10.1016/j.heliyon.2021.e06459
9. K. J. Wang, The generalized (3+1)-dimensional B-type Kadomtsev-Petviashvili equation: Resonant multiple soliton, N-soliton, soliton molecules and the interaction solutions, *Nonlinear Dyn.*, **112** (2024), 7309–7324. https://doi.org/10.1007/s11071-024-09356-7
10. H. H. Hussein, H. M. Ahmed, W. Alexan, Analytical soliton solutions for cubic-quartic perturbations of the Lakshmanan-Porsezian-Daniel equation using the modified extended tanh function method, *Ain Shams Eng. J.*, **15** (2024), 102513. https://doi.org/10.1016/j.asej.2023.102513
11. K. J. Wang, A fast insight into the optical solitons of the generalized third-order nonlinear Schrödinger equation, *Results Phys.*, **40** (2022), 105872. https://doi.org/10.1016/j.rinp.2022.105872
12. Y. H. Liang, K. J. Wang, Dynamics of the new exact wave solutions to the local fractional Vakhnenko-Parkes equation, *Fractals*, 2025, 2550102. https://doi.org/10.1142/S0218348X25501026
13. E. H. Abdullah, A. A. Zaghrout, H. M. Ahmed, A. I. A. Bahnasy, W. B. Rabie, Soliton dynamics and travelling wave solutions for high-order nonlinear Schrödinger equation in birefringent fibers using improved modified extended tanh function method, *Opt. Quant. Electron.*, **56** (2024), 789. https://doi.org/10.1007/s11082-024-06488-3

14. M. B. Almatrafi, Solitary wave solutions to a fractional-order Fokas equation via the improved modified extended tanh-function approach, *Mathematics*, **13** (2025), 109. https://doi.org/10.3390/math13010109
15. Z. Yang, B. Y. C. Hon, An improved modified extended tanh-function method, *Z. Naturforsch. A*, **61** (2006), 103–115. https://doi.org/10.1515/zna-2006-3-401
16. A. A. Mamun, S. N. Ananna, P. P. Gharami, T. An, M. Asaduzzaman, The improved modified extended tanh-function method to develop the exact travelling wave solutions of a family of 3D fractional WBBM equations, *Results Phys.*, **41** (2022), 105969. https://doi.org/10.1016/j.rinp.2022.105969
17. C. Gomez, An effective fractional paraxial wave equation for wave-fronts in randomly layered media with long-range correlations, *Multiscale Model. Simul.*, **21** (2023), 1410–1456. https://doi.org/10.1137/22M1525594
18. G. Akram, M. Sadaf, S. Arshed, M. S. Riaz, Exact solutions of paraxial equation via extended hyperbolic function method, *Opt. Quant. Electron.*, **56** (2024), 1621. https://doi.org/10.1007/s11082-024-07490-5
19. S. Tarla, R. Yilmazer, Investigation of time-dependent paraxial equation with an analytical method, *Optik*, **261** (2022), 169111. https://doi.org/10.1016/j.ijleo.2022.169111
20. S. Tarla, K. K. Ali, R. Yilmazer, Newly modified unified auxiliary equation method and its applications, *Optik*, **269** (2022), 169880. https://doi.org/10.1016/j.ijleo.2022.169880
21. Abdullah, G. U. Rahman, O. Tunc, Analytical optical soliton solution & stability analysis of the dimensionless time-dependent paraxial equation, *Indian J. Phys.*, **99** (2025), 4181–4195. https://doi.org/10.1007/s12648-025-03614-z
22. S. Ramzan, M. Arshad, A. R. Seadawy, I. Ahmed, N. Hussain, Studying exploring paraxial wave equation in Kerr media: Unveiling the governing laws, rational solitons and multi-wave solutions and their stability with applications, *Mod. Phys. Lett. B*, **39** (2025), 2450513. https://doi.org/10.1142/S0217984924505134
23. K. J. Wang, H. W. Zhu, S. Li, F. Shi, G. Li, X. L. Liu, Bifurcation analysis, chaotic behaviors, variational principle, Hamiltonian and diverse optical solitons of the fractional complex Ginzburg-Landau model, *Int. J. Theor. Phys.*, **64** (2025), 134. https://doi.org/10.1007/s10773-025-05977-9
24. M. S. Ullah, M. Z. Ali, H. O. Roshid, Bifurcation analysis and new waveforms to the first fractional WBBM equation, *Sci. Rep.*, **14** (2024), 11907. https://doi.org/10.1038/s41598-024-62754-0
25. K. Hosseini, E. Hinal, M. Ilie, Bifurcation analysis, chaotic behaviors, sensitivity analysis, and soliton solutions of a generalized Schrödinger equation, *Nonlinear Dyn.*, **111** (2023), 17455–17462. https://doi.org/10.1007/s11071-023-08759-2
26. S. Zhao, Multiple solutions and dynamical behavior of the periodically excited beta-fractional generalized KdV-ZK system, *Phys. Scr.*, **100** (2025), 045244. https://doi.org/10.1088/1402-4896/adc20c

AIMS Press